Monatsh Chem (2010) 141:1–6
DOI 10.1007/s00706-009-0224-5

ORIGINAL PAPER

$La_6Pd_{13}Cd_4$ and $Ce_6Pd_{13}Cd_4$ with palladium-centred rare earth octahedra: synthesis, structure, and chemical bonding

Frank Tappe · Samir F. Matar · Rainer Pöttgen

Received: 29 October 2009 / Accepted: 19 November 2009 / Published online: 15 December 2009

Abstract The palladium-rich cadmium compounds $La_6Pd_{13}Cd_4$ and $Ce_6Pd_{13}Cd_4$ were synthesized by induction melting the elements in sealed tantalum ampoules and subsequent annealing. They were characterized by X-ray powder and single-crystal diffraction: $Na_{16}Ba_6N$ type, $Im\bar{3}m$, $a = 988.12(9)$ pm, $wR2 = 0.0463$, 225 F^2 values, and 12 variables for $La_6Pd_{13}Cd_4$, and $a = 982.1(2)$ pm, $wR2 = 0.0521$, 215 F^2 values, and 12 variables for $Ce_6Pd_{13}Cd_4$. The striking structural motifs are palladium-centred La_6 and Ce_6 octahedra, which are packed in a *bcc* fashion. Further palladium and cadmium atoms built up three-dimensional $[Pd_3Cd]$ networks in which the La_6Pd and Ce_6Pd octahedra are embedded. Chemical bonding analyses show that the dominant interaction occurs within the palladium-centred RE_6 octahedra, while weaker bonding exists between them.

Keywords Cadmium compounds · Crystal chemistry · Electronic structure calculation

Introduction

Ternary intermetallic $RE_xT_yCd_z$ compounds [*RE*: rare earth metal; *T*: late transition metal] often show strong crystal chemical similarities to $RE_xT_yMg_z$ compounds [1]. Typical examples include the equiatomic compounds *RETCd* [2–5], the Mo_2FeB_2-type compounds RE_2T_2Cd [6, 7, and references therein], and the series of rare earth metal-rich compounds RE_4TCd [8–10] and $RE_{23}T_7Cd_4$ [11, 12]. A common structural motif of all of these compounds are transition metal-centred trigonal prisms of the rare earth elements. These prisms show peculiar connectivity patterns for each structure type. The *RE–T* distances within the trigonal prismatic units are close to the sums of the covalent radii, and one observes strong covalent *RE–T* bonding.

During recent phase-analytical studies of *RE–T–*Cd systems, we discovered an exceptional compound, $Pr_6Pd_{13}Cd_4$ [13], which crystallizes with a site occupancy variant of the structure of the subnitride $Na_{16}Ba_6N$ [14]. In contrast to all other $RE_xT_yCd_z$ compounds, $Pr_6Pd_{13}Cd_4$ shows discrete, palladium-centred Pr_6Pd octahedra which are arranged in a body-centred cubic packing system. We have now also observed this structure type for the lanthanum and the cerium compound. The synthesis, structure refinements and chemical bonding peculiarities of $La_6Pd_{13}Cd_4$ and $Ce_6Pd_{13}Cd_4$ are reported herein.

Results and discussion

Structure refinement

Careful analysis of the diffractometer data sets revealed body-centred cubic lattices and no further extinctions. In agreement with our previous investigations on $Pr_6Pd_{13}Cd_4$ [13], the space group $Im\bar{3}m$ was found to be correct during the structure refinements. The atomic parameters of $Pr_6Pd_{13}Cd_4$ [13] were taken as starting values and both structures were refined using Shelxl-97 [15] (full-matrix

F. Tappe · R. Pöttgen (✉)
Institut für Anorganische und Analytische Chemie,
Westfälische Wilhelms-Universität Münster,
Corrensstrasse 30, 48149 Münster, Germany
e-mail: pottgen@uni-muenster.de

S. F. Matar
CNRS, ICMCB, Université de Bordeaux,
87 Avenue du Docteur Albert Schweitzer,
33608 Pessac Cedex, France

Table 1 Crystal data and structure refinement for $La_6Pd_{13}Cd_4$ and $Ce_6Pd_{13}Cd_4$, space group $Im\bar{3}m$, $Z = 2$

Empirical formula	$La_6Pd_{13}Cd_4$	$Ce_6Pd_{13}Cd_4$
Formula weight (g/mol)	2,666.26	2,673.52
Unit cell dimensions (pm)	$a = 988.12(9)$	$a = 982.1(2)$
Cell volume (nm^3)	$V = 0.9648$	$V = 0.9473$
Calculated density (g/cm^3)	9.18	9.37
Crystal size (μm^3)	$10 \times 20 \times 60$	$20 \times 20 \times 40$
Transmission ratio (max/min)	0.744/0.391	0.576/0.307
Absorption coefficient (per mm)	29.0	30.4
$F(000)$	2,264	2,276
Detector distance (mm)	60	70
Exposure time (min)	4	3
ω range; increment (°)	0–180, 1.0	0–180, 1.0
Integration parameters A, B, EMS	13.5, 3.5, 0.012	13.5, 3.5, 0.012
θ range for data collection (°)	2–34	2–34
Range in hkl	±15, ±15, ±15	±15, ±15, ±15
Total no. of reflections	7253	6583
Independent reflections	225 ($R_{int} = 0.1366$)	215 ($R_{int} = 0.0466$)
Reflections with $I \geq 2\sigma(I)$	157 ($R_{sigma} = 0.0636$)	173 ($R_{sigma} = 0.0217$)
Data/parameters	225/12	215/12
Goodness-of-fit on F^2	0.843	0.992
Final R indices [$I \geq 2\sigma(I)$]	$R1 = 0.0278$	$R1 = 0.0238$
	$wR2 = 0.0419$	$wR2 = 0.0481$
R indices (all data)	$R1 = 0.0636$	$R1 = 0.0401$
	$wR2 = 0.0463$	$wR2 = 0.0521$
Extinction coefficient	0.00112(6)	0.00070(7)
Largest diff. peak and hole ($e/Å^3$)	2.48 and −2.06	3.73 and −2.11

Table 2 Atomic coordinates and isotropic displacement parameters (pm^2) for $La_6Pd_{13}Cd_4$ and $Ce_6Pd_{13}Cd_4$. U_{eq} is defined as one-third of the trace of the orthogonalized U_{ij} tensor

Atom	Wyckoff position	x	y	z	U_{eq}
$La_6Pd_{13}Cd_4$					
La	12*e*	0.30403(12)	0	0	55(3)
Pd1	2*a*	0	0	0	81(8)
Pd2	24*h*	0	0.33904(7)	*y*	72(2)
Cd	8*c*	1/4	1/4	1/4	78(3)
$Ce_6Pd_{13}Cd_4$					
Ce	12*e*	0.30338(9)	0	0	68(2)
Pd1	2*a*	0	0	0	90(5)
Pd2	24*h*	0	0.34010(6)	*y*	74(2)
Cd	8*c*	1/4	1/4	1/4	87(3)

least-squares on F^2) with anisotropic atomic displacement parameters for all atoms. To check for the correct composition, the occupancy parameters were refined in separate series of least-squares cycles. All sites were fully occupied within two standard deviations, and in the final cycles the ideal occupancies were assumed again. The final difference Fourier syntheses were flat (Table 1). The positional parameters and interatomic distances of the refinements are listed in Tables 2 and 3. Further information on the structure refinements is available (see the "Experimental" section).

Crystal chemistry

New ternary cadmium compounds $La_6Pd_{13}Cd_4$ and $Ce_6Pd_{13}Cd_4$ crystallize with a site occupancy variant of the subnitride $Na_{16}Ba_6N$ [14], similar to $Pr_6Pd_{13}Cd_4$ [13]. The cubic lattice parameter decreases from the lanthanum to the praseodymium compound, as expected from the lanthanoid contraction. A view of the $La_6Pd_{13}Cd_4$ structure approximately along the *c* axis is presented in Fig. 1. The striking structural motifs of the $La_6Pd_{13}Cd_4$ structure are Pd1-centred La_6 octahedra, which are packed in a *bcc* arrangement. These correspond to the Ba_6N octahedra in the subnitride $Na_{16}Ba_6N$ [14]. In both structures the octahedra are well separated from each other. They are embedded in a matrix of sodium atoms in $Na_{16}Ba_6N$ and within an ordered $[Pd_3Cd]$ network in $La_6Pd_{13}Cd_4$ (Fig. 2).

Table 3 Interatomic distances (pm) for $La_6Pd_{13}Cd_4$ and $Ce_6Pd_{13}Cd_4$ (calculated with the powder lattice parameters). All of the distances of the first coordination spheres are listed

$La_6Pd_{13}Cd_4$				$Ce_6Pd_{13}Cd_4$			
La:	4	Pd2	296.8	Ce:	4	Pd2	294.3
	1	Pd1	300.4		1	Pd1	297.9
	6	Pd2	336.8		6	Pd2	336.0
	4	Cd	353.4		4	Cd	351.2
	1	La	387.3		1	Ce	386.2
	4	La	424.9		4	Ce	421.4
Pd1:	6	La	300.4	Pd1:	6	Ce	297.9
Pd2:	2	Cd	276.6	Pd2:	2	Cd	275.6
	4	Pd2	285.6		4	Pd2	284.0
	2	La	296.8		2	Ce	294.3
	2	Pd2	318.1		2	Pd2	314.1
	2	La	336.8		2	Ce	336.0
Cd:	6	Pd2	276.6	Cd:	6	Pd2	275.6
	6	La	353.4		6	Ce	351.2

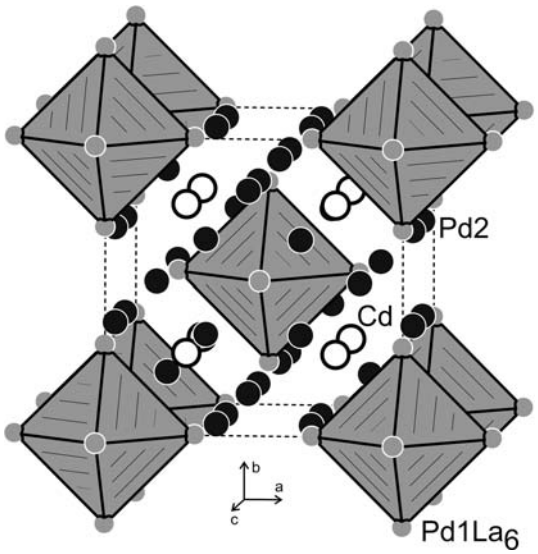

Fig. 1 The crystal structure of cubic $La_6Pd_{13}Cd_4$. Lanthanum, palladium, and cadmium atoms are drawn as *medium grey*, *black*, and *open circles*, respectively. The palladium-centred La_6 octahedra are emphasized

The La–Pd1 distances within the octahedra of 300 pm are close to the sum of the covalent radii [16] of 297 pm, and we can assume that substantial La–Pd bonding occurs in these monomer units. Similar short La–Pd distances occur in the binary compounds $LaPd_3$ (Cu_3Au type, 12 × 300 pm La–Pd) [17] and $LaPd_5$ ($CaCu_5$ type, 6 × 306 pm La–Pd) [18]. Palladium-centred trigonal prisms and octahedra of rare earth elements are a common structural motif in various ternary compounds. Table 4 summarizes the single-crystal data for the palladium-based compounds that have such data available for them.

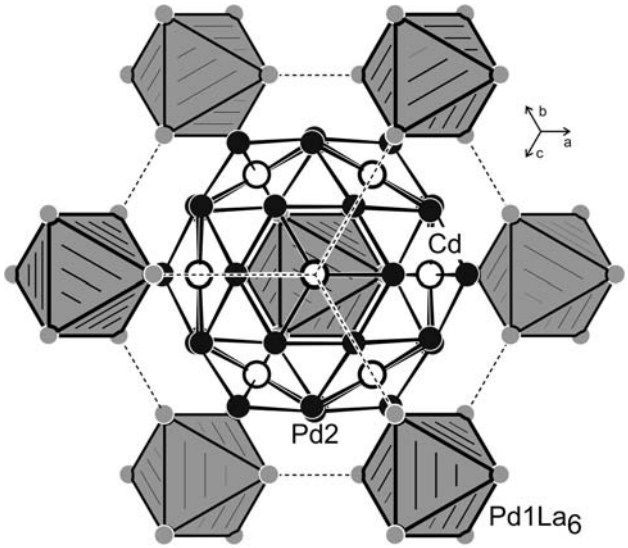

Fig. 2 Projection of the $La_6Pd_{13}Cd_4$ structure along the threefold axis. Lanthanum, palladium, and cadmium atoms are drawn as *medium grey*, *black*, and *open circles*, respectively. The isolated $Pd1La_6$ octahedra and the three-dimensional $[Pd_3Cd]$ network are emphasized

Table 4 *RE*–Pd distances (pm) in the trigonal prismatic (tp) and octahedral (o) RE_6T units in selected ternary intermetallic compounds

Compound	Motif	Distances	Reference
Gd_4PdCd	tp	287, 288	[10]
Gd_4PdMg	tp	287, 289	[21]
Ce_2Pd_2Mg	tp	293–309	[22]
Nd_2Pd_2Cd	tp	291–305	[19]
$Er_{14}Pd_3In_3$	tp	276–287	[20]
$La_6Pd_{13}Cd_4$	o	300	This work
$Ce_6Pd_{13}Cd_4$	o	298	This work
$Pr_6Pd_{13}Cd_4$	o	296	[13]

Within the $[Pd_3Cd]$ network embedding the $Pd1La_6$ octahedra, the Pd2–Cd distances of 277 pm are only slightly longer than the sum of the covalent radii of 269 pm [16]. The Pd2–Pd2 distances of 286 pm are comparable to *fcc* palladium (275 pm) [23]. Bonding of the $Pd1La_6$ octahedra to the $[Pd_3Cd]$ network proceeds via four short La–Pd2 contacts at 297 pm. The shortest La–Cd distance of 353 pm is significantly longer than the sum of the covalent radii of 310 pm [16]. A more quantitative view of the bonding peculiarities is given in the following section.

Chemical bonding analyses

At self-consistent convergence, little charge transfer was observed between the atoms for both intermetallic compounds. It can be argued that the quantum mixing between

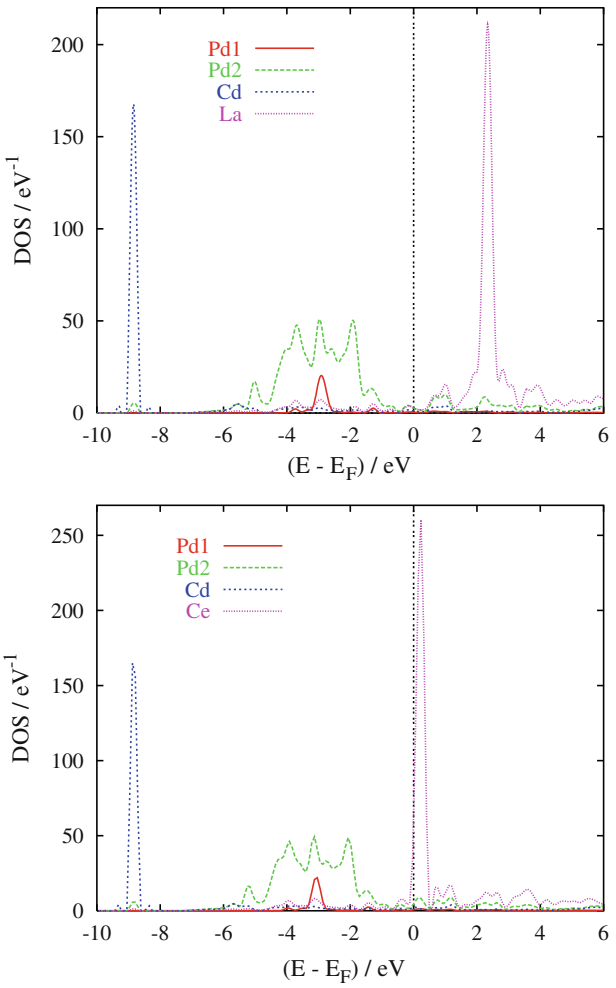

Fig. 3 Site projected densities of states (*PDOS*) of $La_6Pd_{13}Cd_4$ (*top*) and $Ce_6Pd_{13}Cd_4$ (*bottom*)

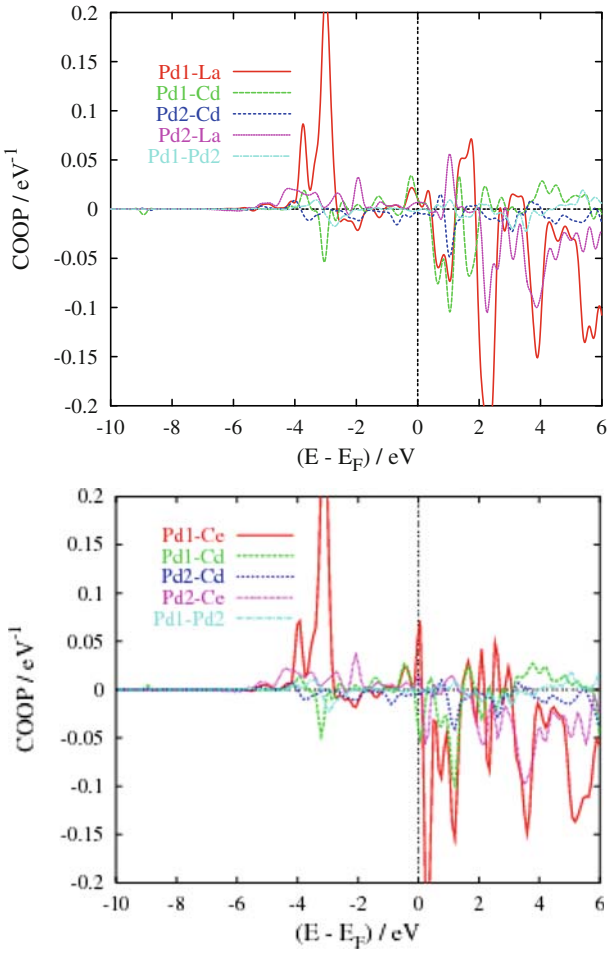

Fig. 4 Chemical bonding (*COOP*) within $La_6Pd_{13}Cd_4$ (*top*) and $Ce_6Pd_{13}Cd_4$ (*bottom*)

the different valence states of the constituents is the underlying mechanism of bonding, as will be shown first from the site projected density of states (PDOS), and then from an analysis of the chemical bonding based on overlap populations (COOP).

Figure 3 shows the PDOS for $La_6Pd_{13}Cd_4$ and $Ce_6Pd_{13}Cd_4$. The multiplicity of the atoms is accounted for by separating the Pd into 1 Pd1 and 12 Pd2. The Fermi level (E_F) is taken as zero energy. This is also done in the following plots describing the chemical bonding. Both plots show a similar valence band (VB) with low-lying Cd $4d^{10}$ states at -9 eV and Pd 4*d* states in the energy window -6, -1 eV. Despite the 1/12 intensity ratio, it can be seen that Pd1 states show strong localization around -3 eV with itinerant *RE* PDOS present below the peak. This will be shown to have an effect on the strength of the chemical bonding. E_F crosses low-intensity itinerant-like DOS with empty La 4*f* states found above, as expected. In the cerium compound, the Fermi level crosses the lower part of the Ce 4*f* states (one more electron vs. La) with a rather high intensity, which could indicate a possible magnetic instability leading to the onset of finite magnetic polarization. Our calculations resulted in a magnetic moment of 0.76 μ_B per cerium atom (spin only value). Unfortunately, all of our $Ce_6Pd_{13}Cd_4$ samples contained approximately 10% (estimated based on the Guinier data) $CePd_3$. This Cu_3Au-type compound [24] exhibits intermediate-valent cerium [25]. Due to the $CePd_3$ by-product, an experimental study of the magnetic data was not reasonable.

Figure 4 details the atom-to-atom (one-to-one) interaction within both intermetallic compounds. The major part of the VB is found to exhibit a bonding character (positive *y*-magnitudes) for the different interactions, which are all of low magnitude, except for Pd1–*RE*, which is found to prevail. In the lower part of the VB, no bonding arising from Cd 4*d* states is seen, which are thus inactive. The large COOP peak at -3 eV follows the observation above of the PDOS peak at this energy (i.e. it involves itinerant states of the rare earth atoms

and Pd1). The antibonding counterpart (negative *y*-magnitude) is found above E_F, at 2 eV. In the Ce compound there is a bonding contribution from 4*f*–4*d* of Ce and Pd1.

Experimental

Synthesis

Starting materials for the preparation of the $La_6Pd_{13}Cd_4$ and $Ce_6Pd_{13}Cd_4$ samples were sublimed ingots of lanthanum and cerium (Johnson Matthey and Smart Elements), palladium powder (Heraeus, ca. 200 mesh) and a cadmium rod (Johnson Matthey), all with stated purities of better than 99.9%. Small pieces of the lanthanum and cerium ingots (~300 mg) were first arc-melted [26] to small buttons under an argon atmosphere of ca. 800 mbar. Argon was purified with a titanium sponge (900 K), silica gel, and molecular sieves. The rare earth buttons, palladium powder, and pieces of the cadmium rod were then mixed in an atomic ratio of 6:13:4 under flowing argon and arc-welded [26] in tantalum ampoules under an argon pressure of about 700 mbar.

The tubes were then placed in a water-cooled sample chamber [27] of an induction furnace and heated twice at ca. 1,470 K for a period of 5 min followed by quenching. The samples were then broken off the tubes (no reaction with the container material was observed) and the powder patterns showed mainly $LaPd_3$ and $CePd_3$ with Cu_3Au-type structure. The crushed products were then finely ground to powders in an agate mortar, cold-pressed into small pellets (∅ 6 mm), sealed in evacuated silica ampoules, and annealed at 920 K in a muffle furnace for 4 weeks. We then obtained the $RE_6Pd_{13}Cd_4$ compounds in high yield along with small amounts of the by-products $LaPd_3$ and $CePd_3$. The resulting samples were quite brittle. They are stable in air. Single crystals exhibit a metallic lustre, while powders are dark grey.

Scanning electron microscopy

Semiquantitative EDX analyses of the bulk samples and the single crystals measured on the diffractometer were carried out using a Leica 420i scanning electron microscope with LaF_3, CeO_2, palladium, and cadmium employed as standards. The crystals, mounted on quartz fibres, were first coated with a thin carbon film to ensure conductivity. No impurity elements heavier than sodium (detection limit of the instrument) were detected. The experimentally determined compositions were close to the ideal ones.

X-ray data collection

The polycrystalline $La_6Pd_{13}Cd_4$ and $Ce_6Pd_{13}Cd_4$ samples were studied by obtaining their Guinier powder patterns (imaging plate technique, Fujifilm BAS–1800) using $CuK\alpha_1$ radiation and α-quartz ($a = 491.30$ and $c = 540.46$ pm) as an internal standard. The cubic lattice parameters (Table 1) were obtained from least-squares fits of the powder data. To ensure correct indexing, the experimental patterns were compared to calculated ones [28], with the atomic positions taken from the structure refinements (Table 1). The powder and single-crystal lattice parameters agreed well.

Well-shaped single crystals of $La_6Pd_{13}Cd_4$ and $Ce_6Pd_{13}Cd_4$ were selected from the annealed samples and investigated via Laue photographs on a Buerger camera (white Mo radiation), equipped with the same Fujifilm, BAS-1800 imaging plate technique, in order to check the quality for intensity data collection. Intensity data were collected on a Stoe IPDS II diffractometer (graphite monochromatized MoKα radiation; oscillation mode), and numerical absorption corrections were applied to the data sets. All relevant details concerning the data collections and evaluations are listed in Table 1. Further information on the structure refinements may be obtained from Fachinformationszentrum Karlsruhe, D-76344 Eggenstein-Leopoldshafen (Germany), by quoting the Registry Nos. CSD–421178 ($La_6Pd_{13}Cd_4$) and CSD–421179 ($Ce_6Pd_{13}Cd_4$).

Computational details

Electronic structure calculations were performed for both intermetallic compounds using the scalar relativistic full-potential augmented spherical wave (ASW) method [29, 30] built within the density functional theory (DFT) framework [31, 32]. All valence states including Cd $4d^{10}$ and *RE* 4*f* were treated as band states. In the minimal ASW basis set, the outermost shells were chosen to represent the valence states using partial waves up to $l_{max} + 1 = 4$ for La and Ce, and $l_{max} + 1 = 3$ for Pd and Cd. The completeness of the valence basis set was checked for charge convergence (i.e. less than 0.1 electrons for $l_{max} + 1$). The self-consistent field calculations were run to a convergence level of 10^{-8} for the charge density, and the accuracy of the method is in the range of about 10^{-8} Ryd (1 Ryd = 13.6 eV) regarding energy differences. The effects of exchange and correlation were treated based on the local density approximation LDA [33]. Spin-degenerate, nonmagnetic (NM) calculations were carried out for the analysis of PDOS and the chemical bonding based on the COOP scheme introduced by Hoffmann [34] in extended Hückel-type calculations. In shorthand notation,

avoiding extended equations, the COOP can be considered the DOS weighted by the overlap integral S_{ij} between two chemical species i and j. This has the same units as the DOS of inverse energy (1/eV). In the plots, positive, negative, and zero magnitudes of COOP are indicative of bonding, antibonding, and nonbonding interactions, respectively.

Acknowledgments This work was financially supported by the Deutsche Forschungsgemeinschaft. We are thankful to Dipl.-Ing. U. Ch. Rodewald for the intensity data collections. The computations benefited from the M3PEC-Mesocentre/University Bordeaux 1 facility.

References

1. Rodewald UC, Chevalier B, Pöttgen R (2007) J Solid State Chem 180:1720
2. Iandelli A (1992) J Alloys Compd 182:87
3. Horechyy AI, Pavlyuk VV, Bodak OI (1999) Pol J Chem 73:1681
4. Pavlyuk VV, Horechyj AI, Kevorkov DG, Dmytriv GS, Bodak OI, Koziol JJ, Ciesielski W, Kapuśniak J (2000) J Alloys Compd 296:276
5. Mishra R, Pöttgen R, Hoffmann R-D, Kaczorowski D, Piotrowski H, Mayer P, Rosenhahn C, Mosel BD (2001) Z Anorg Allg Chem 627:1283
6. Lukachuk M, Pöttgen R (2003) Z Kristallogr 218:767
7. Schappacher FM, Hermes W, Pöttgen R (2009) J Solid State Chem 182:265
8. Doğan A, Rayaprol S, Pöttgen R (2007) J Phys Condens Matter 19:076213
9. Schappacher FM, Pöttgen R (2008) Monatsh Chem 139:1137
10. Schappacher FM, Rodewald UC, Pöttgen R (2008) Z Naturforsch 63B:1127
11. Tappe F, Pöttgen R (2009) Z Naturforsch 64B:184
12. Tappe F, Hermes W, Eul M, Pöttgen R (2009) Intermetallics 17:1035
13. Doğan A, Hoffmann R-D, Pöttgen R (2007) Z Anorg Allg Chem 633:219
14. Snyder GJ, Simon A (1994) Angew Chem 106:713
15. Sheldrick GM (1997) Shelxl-97: program for crystal structure refinement. University of Göttingen, Göttingen
16. Emsley J (1999) The elements. Oxford University Press, Oxford
17. Dwight AE, Downey JW, Conner RA Jr (1961) Acta Crystallogr 14:75
18. Yuan-Tao N, Xin-Ming Z, Yun Z, Nian-Yi C, Hua X, Jian-Zhong Z (1989) J Less Common Met 147:167
19. Rayaprol S, Doğan A, Pöttgen R (2006) J Phys Condens Matter 18:5473
20. Zaremba R, Rodewald UC, Pöttgen R (2007) Z Naturforsch 62B:1574
21. Tuncel S, Chevalier B, Pöttgen R (2008) Z Naturforsch 63B:600
22. Pöttgen R, Fugmann A, Hoffmann R-D, Rodewald UC, Niepmann D (2000) Z Naturforsch 55B:155
23. Donohue J (1974) The structures of the elements. Wiley, New York
24. Harris IR, Raynor GV (1965) J Less Common Met 9:263
25. Hutchens RD, Rao VUS, Greedan JE, Wallace WE, Craig RS (1971) J Appl Phys 42:1293
26. Pöttgen R, Gulden T, Simon A (1999) GIT Labor Fachzeitschrift 43:133
27. Kußmann D, Hoffmann R-D, Pöttgen R (1998) Z Anorg Allg Chem 624:1727
28. Yvon K, Jeitschko W, Parthé E (1977) J Appl Crystallogr 10:73
29. Williams AR, Kübler J, Gelatt CD (1979) Phys Rev B 19:6094
30. Eyert V (2007) The augmented spherical wave method: a comprehensive treatment (Lect Notes Phys 719). Springer, Berlin
31. Hohenberg P, Kohn W (1964) Phys Rev 136:B864
32. Kohn W, Sham LJ (1965) Phys Rev 140:A1133
33. Vosko SH, Wilk L, Nusair M (1980) Can J Phys 58:1200
34. Hoffmann R (1987) Angew Chem Int Ed 26:846